Applied Catalysis A: General 477 (2014) 102–108

Contents lists available at ScienceDirect

Applied Catalysis A: General

journal homepage: www.elsevier.com/locate/apcata

Ordered mesoporous tungsten carbide nanoplates as non-Pt catalysts for oxygen reduction reaction

A-Ra Ko[a,1], Young-Woo Lee[a,1], Je-Suk Moon[a,1], Sang-Beom Han[a], Guozhong Cao[b], Kyung-Won Park[a,*]

[a] Department of Chemical Engineering, Soongsil University, Seoul 156743, Republic of Korea
[b] Department of Materials Science and Engineering, University of Washington, Seattle, WA 98195, USA

ARTICLE INFO

Article history:
Received 26 August 2013
Received in revised form 22 February 2014
Accepted 26 February 2014
Available online 13 March 2014

Keywords:
Mesoporous
Tungsten carbide
Palladium
Oxygen reduction reaction
Electrochemical properties

ABSTRACT

We represent well-defined mesoporous tungsten carbide catalysts for oxygen reduction reaction in alkaline solution. The pore structures of tungsten carbide nanoplates (WC-700-m, WC-800-m and WC-900-m) are formed as a function of reaction temperature of 700, 800 and 900 °C in CH_4(25%)/H_2(75%) atmosphere for 9 h using layered tungsten nitride nanoparticles. All the tungsten carbide nanoplates exhibit isothermal sorption characteristics of mesoporous structure and fairly monomodal pore size distribution in the range of 6.6–7.2 nm. The WC-700-m, WC-800-m, and WC-900-m exhibit X-ray diffraction patterns corresponding to WC_{1-x}, WC_{1-x} + WC, and WC phase, respectively. In particular, the WC-900-m shows highly improved electrocatalytic activity toward oxygen reduction reaction in an alkaline solution as compared to the WC-900-c. Furthermore, the WC-900-m supported Pd catalyst as a non-Pt exhibits much enhanced electrochemical oxygen reduction properties in comparison with conventional Pt catalyst.

1. Introduction

Transition metal carbides have potential applications due to their special properties, such as high melting point, superior hardness, high oxidation resistance, and good electrical conductivity. In particular, they exhibit a well-known catalytic action on the process of oxidation of hydrogen in acidic media having a particular chemical stability and the more resistant poisoning agents [1]. For transition metal carbides to mimic the catalytic properties of Pt-group metals, Levy and Boudart et al. suggested that tungsten carbides displayed Pt-like behavior in catalytic reactions [2–4]. Although the catalytic efficiency of WC is much lower than that of noble metals, a considerable interest has been received in fuel cells for the development of inexpensive systems [5–15]. However, there is a lack of fundamental understanding and conflict between results from different groups regarding the active phases and stability of this class of materials. Since the transition metal carbide components are easily agglomerated under high temperature reaction condition, most of these studies were carried out on low surface area materials.

The synthetic methods for high surface area carbides include gas-phase reactions of metal compounds, reaction of gaseous reagents with solid-state metal compounds, pyrolysis of metal precursors and solution reactions [16–19]. Boudart et al. developed a temperature programmed reaction method, which an oxide precursor is placed in a CH_4 gas atmosphere with increasing temperature [20]. In particular, mesoporous structure materials have received interests because of their wide range of potential applications such as separation, sensors, and, in particular, catalysis [21–24]. A key issue for improving this class of mesoporous structure is the development of synthesis methods that produce materials with high surface areas and controlled pore sizes in the nanometer range [25–30]. Recently, several mesoporous materials synthesized by neutral templating and ligand-assisted templating methods have been reported [31–36]. Through well-developed template methods, conventional template method is difficult to apply for the preparation of ordered mesoporous self-supported metal carbides. Until now, there have been few reports regarding the synthesis of self-supported ordered mesoporous transition metal carbides with mono-modal distribution of pore size.

Here we prepared well-defined mesoporous tungsten carbides by means of template-free synthesis using layered tungsten nitride nanoparticles. The mesoporous tungsten carbides were characterized by field-emission scanning electron microscopy (FE-SEM), field-emission transmission electron microscopy (FE-TEM), X-ray

* Corresponding author. Tel.: +82 2 820 0613; fax: +82 2 812 5378.
E-mail address: kwpark@ssu.ac.kr (K.-W. Park).
[1] All authors contributed equally to this work.

http://dx.doi.org/10.1016/j.apcata.2014.02.034
0926-860X/

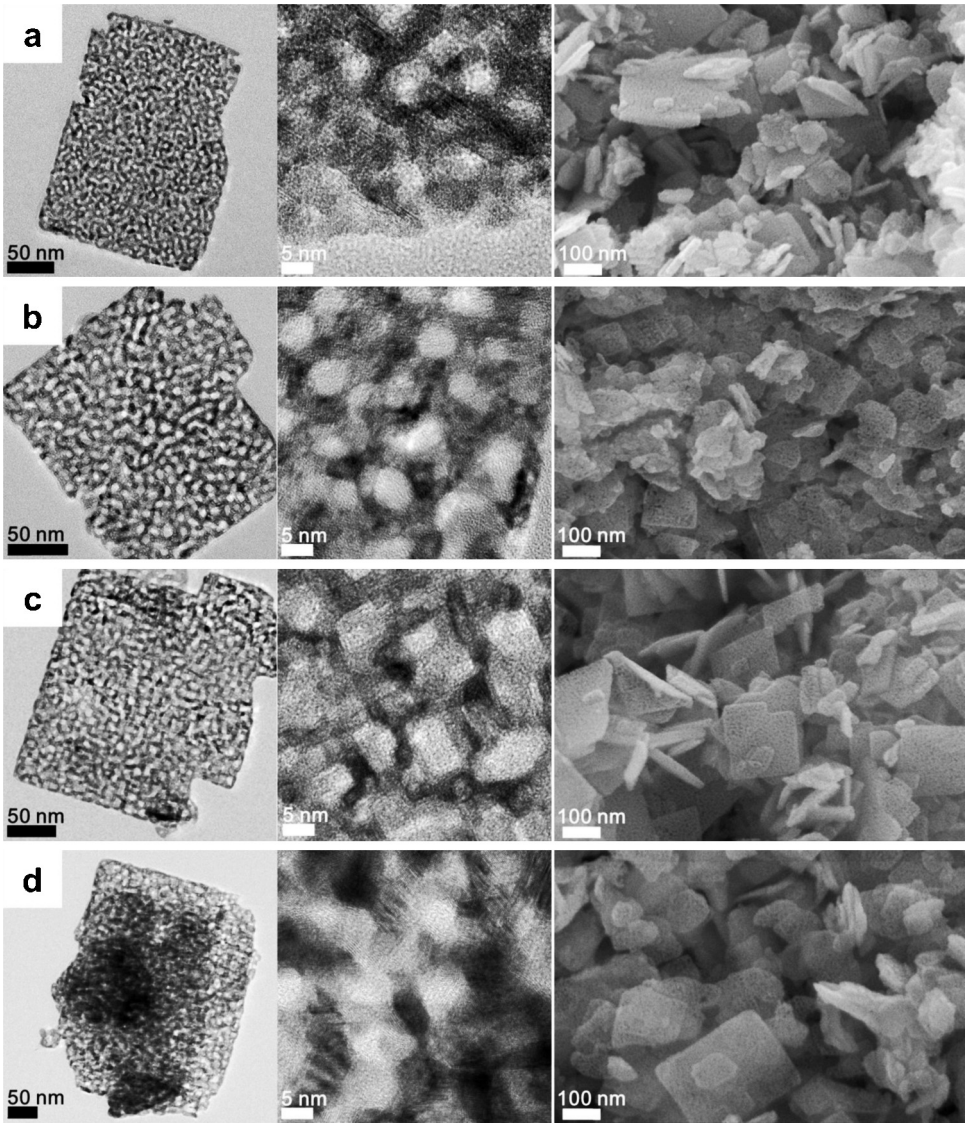

Fig. 1. TEM and SEM images of (a) as-prepared W_2N nanoparticles and samples prepared at (b) 700 °C and (c) 800 °C, and (d) 900 °C in CH_4/H_2 mixture using W_2N nanoparticles.

powder diffraction (XRD), and X-ray photoelectron spectroscopy (XPS). The surface area and porosity of the synthesized samples were analyzed by a nitrogen sorption measurement. To evaluate the performance of the catalysts in oxygen reduction reaction (ORR), cyclic voltammograms (CVs) and linear sweep voltammograms were obtained in comparison with Pt/C catalyst using a potentiostat.

2. Experimental

2.1. Synthesis of mesoporous tungsten carbides

To prepare layered tungsten nitride nanoparticles, layered tungsten oxide was prepared by a hydrothermal method. For the layered tungsten oxide particles, ammonium tungstate ($(NH_4)_{10}H_2(W_2O_7)_6$) (Aldrich, 99.99%) as a precursor was dissolved in 5 M hydrochloric acid solution (Aldrich, 35%) with constant stirring at 25 °C for 1 h and then kept at 120 °C for 2 h. After the hydrothermal process, the resulting precipitate was cooled to room temperature, washed several times with ethanol and distilled water, and then filtered by using a filtration. The yellow layered tungsten oxide powder was obtained after drying in 50 °C oven. For tungsten nitride structures from tungsten oxides, the resulting powder was loaded into a quartz boat, which was inserted into a vitreous quartz tube inside a cylindrical furnace, heated to reaction temperatures until 700 °C for 1 h, and then maintained at 700 °C for 3 h in the NH_3 of 100 mL min^{-1}. The samples were cooled down to room temperature in flowing NH_3, and passivated for 2 h in an air flow in order to avoid drastic reoxidation to tungsten oxide when they were exposed to air. The as-prepared tungsten nitrides were then loaded into a quartz boat, which was then inserted into a vitreous quartz tube inside a cylindrical furnace. A gas mixture of 25% CH_4/H_2 was passed through the quartz tube at a rate of 100 mL min^{-1} during the entire reaction. Tungsten carbide catalysts studied in this work were prepared at 700, 800, and 900 °C, respectively, (denoted as WC-700-m, WC-800-m, and WC-900-m, respectively). After carburization, all the samples were passivated in an air gas flow for more than 5 h before being removed from quartz tube.

2.2. Preparation of mesoporous tungsten carbide-supported Pd catalysts

For the preparation of WC-900-m supported Pd (4 wt.%) catalyst (denoted as Pd/WC-900-m), the WC-900-m powder was dispersed into anhydrous ethanol and then Na_2PdCl_4 was dissolved in the

solution with continuous stirring for 1 h. After the complete dissolution, $NaBH_4$ solution as a reductant with an excess amount was added to the mixture solution and continuously stirred at 25 °C for 2 h. Finally, the resulting precipitate was washed with de-ionized water and anhydrous ethanol, and dried at 50 °C oven.

2.3. Structural analysis of as-prepared catalysts

The as-prepared samples were characterized by FE-TEM and energy dispersive X-ray (EDX) spectroscopy using a Tecnai G2 F30 system operating at 300 kV. The TEM samples were prepared by placing a drop of the nanoparticle suspension in ethanol on a carbon-coated copper grid. Structural analysis of the mesoporous structures was carried out by XRD method using a Rigaku diffractometer equipped with a Cu K_α radiation source of $\lambda = 0.15418$ nm with a Ni filter. The tube current was 100 mA with a tube voltage of 40 kV. The 2θ between 20° and 80° was explored at a scan rate of 5° min^{-1}. The surface area and porosity of the synthesized samples were analyzed by a nitrogen sorption measurement (Micromeritics ASAP 2020 adsorption analyzer). XPS (Thermo Scientific, K-Alpha) analysis was carried out with the Al K_α X-ray source of 1486.8 eV at the chamber pressure below 1×10^{-8} Torr and 200 W beam power. All high resolution spectra were collected using a pass energy of 46.95 eV. The step size and time per step were chosen to be 0.025 eV and 100 ms, respectively. Both ends of the baseline were set sufficiently far so as not to distort the shape of spectra, including tails. Small variation of the range of the base line did not affect the relative amount of fitted species (less than 1%). The C 1s electron binding energy was referenced at 284.6 eV and a nonlinear least-squares curve-fitting program was employed with a Gaussian–Lorentzian production function.

2.4. Electrochemical analysis of as-prepared catalysts

Electrochemical properties of the catalysts were measured in a three-electrode cell at 25 °C using a potentiostat (CH Instrument, CHI 700C). A Pt wire and Hg/HgO (in saturated NaOH) were used as a counter and reference electrode, respectively. The rotating disk electrode (glassy carbon) as a working electrode was polished with 1, 0.3, and 0.05 μm Al_2O_3 paste and then washed in deionized water. The catalyst ink was prepared by ultrasonically dispersing catalyst powders in an appropriate amount of Millipore water and ethanol. The catalyst ink was dropped 0.7 μL onto a rotating disk electrode. To compare electrochemical properties and ORR activity of the catalysts, CVs and linear sweep voltammetric curves were obtained in 0.1 M NaOH solution. The stability test was carried out by applying linear potential sweeps between −0.4 and +0.1 V for 2,000 cycles with a scan rate of 50 mV s^{-1} in O_2-saturated 0.1 M NaOH solution at 25 °C. The oxygen reduction current–potential curves after the stability test of the catalysts were obtained by sweeping the potential from −0.8 to 0.3 V at a scan rate of 5 mV s^{-1} and rotation disk speed of 1600 rpm. The surface areas in the electrochemical data are on the basis of geometric area of the working electrode.

3. Results and discussion

3.1. Structural characterization of mesoporous tungsten carbides

Fig. 1 shows FE-TEM and FE-SEM images of tungsten carbide particles prepared at different reaction temperatures under CH_4/H_2 mixture atmosphere using the as-prepared W_2N nanoparticles. The as-prepared W_2N for mesoporous tungsten carbide reveals porous structure with fairly uniform and regular mesopores (Fig. 1a). In particular, during nitration process using layered tungsten oxide,

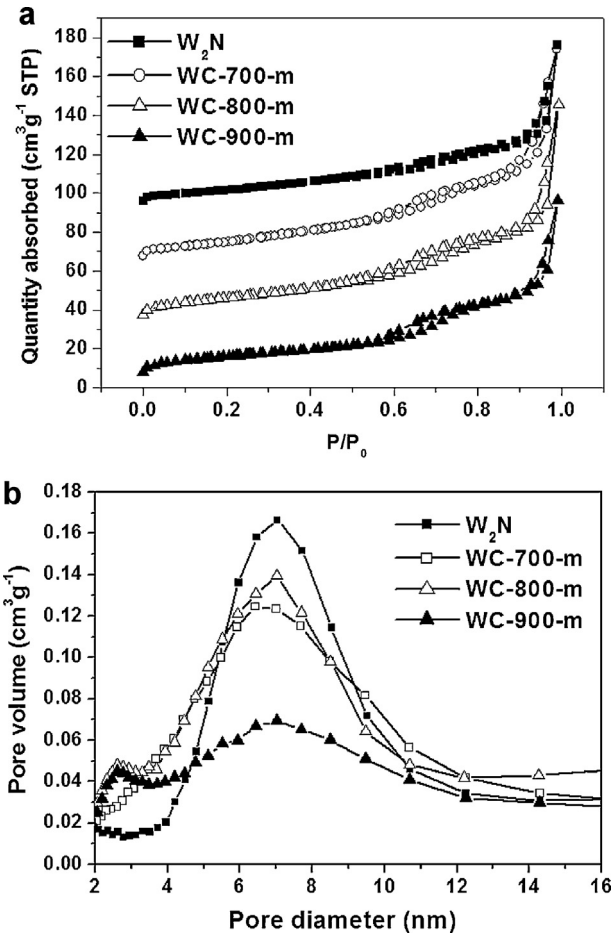

Fig. 2. (a) Nitrogen gas adsorption-desorption isotherms and (b) pore diameter distributions of mesoporous tungsten nitride and tungsten carbide nanoplates.

the W_2N was gradually reduced and then the homogeneous substitution of oxygen vacancies in the reduced oxides with nitrogen atoms occurred. The layered tungsten oxide can offer more open sites forming mesoporous structure. The mesoporous tungsten carbide samples (WC-700-m, WC-800-m, and WC-900-m) were prepared by heating as-prepared W_2N in 25% CH_4 and 75% H_2 atmosphere for 9 h as a function of reaction temperatures.

In order to characterize pore structure of the samples, curves of nitrogen gas adsorption–desorption isotherm and pore size distribution were obtained as shown in Fig. 2 and characteristics of the samples were summarized in Table 1. The as-prepared W_2N exhibits mesoporous structure with 7.2 nm of pore size and 55.6 m^2 g^{-1} of specific surface area. Furthermore, the WC-700-m, WC-800-m, and WC-900-m prepared by the mesoporous W_2N in CH_4/H_2 atmosphere show fairly uniform pore sizes of around 7 nm, which are indicative of mesoporous structure, and specific surface areas of 58.1, 55.2, and 44.5 m^2 g^{-1}, respectively.

Table 1
Comparison of mesoporous tungsten carbides prepared at 700, 800, and 900 °C in CH_4/H_2 mixture using the W_2N nanoparticles.

Sample	Specific surface area (m^2 g^{-1})	Pore diameter (nm)	Phase
W_2N	55.6	7.2	W_2N
WC-700-m	58.1	7.2	WC_{1-x}
WC-800-m	55.2	6.9	WC_{1-x} + WC
WC-900-m	44.6	6.6	WC

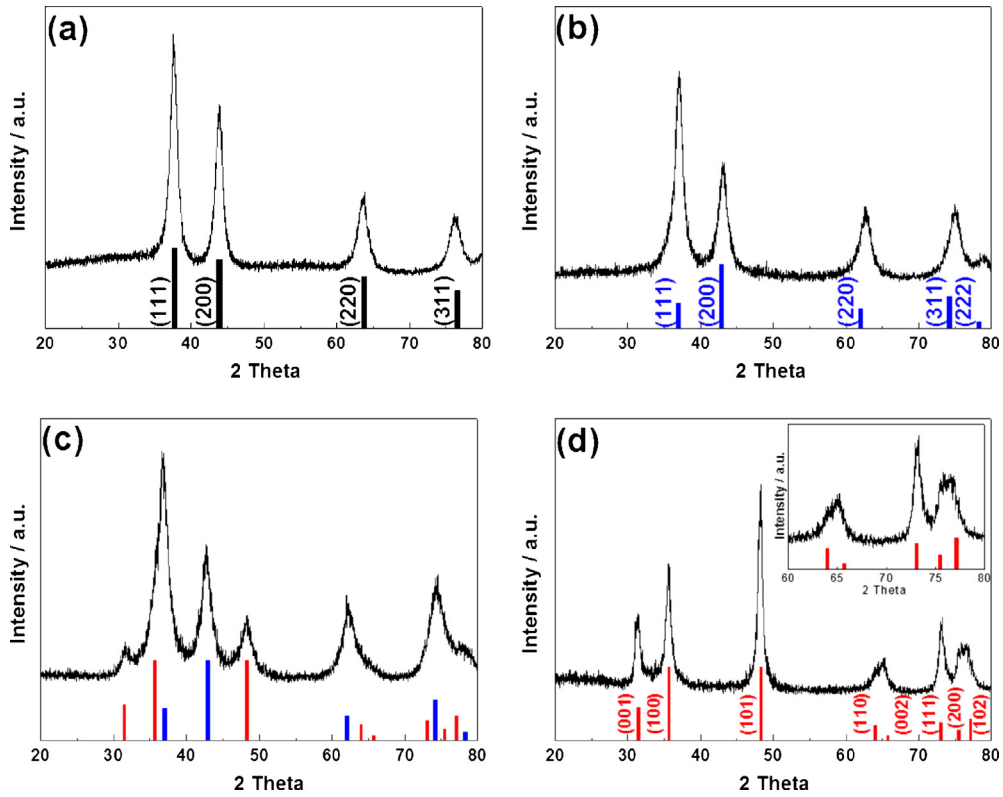

Fig. 3. XRD patterns of (a) as-prepared W_2N, (b) WC-700-m, (c) WC-800-m, and (d) WC-900-m. The inset in Fig. 3d indicates XRD patterns between 60° and 80° of WC-900-m. (XRD reference peaks of W_2N (JCPDS No. 25-1257, black bars, as shown Fig. 3a), WC_{1-x} (JCPDS No. 20-1316, blue bars, as shown Fig. 3b), and WC (JCPDS No. 25-1047, red bars, as shown Fig. 3d)). (For interpretation of the color information in this figure legend, the reader is referred to the web version of the article.)

Fig. 3 shows that XRD patterns of the mesoporous tungsten carbides prepared using W_2N as a function of reaction temperature. The WC-700-m exhibits diffraction patterns of 2θ values at 36.9°, 42.8°, 62.0°, 74.2°, and 78.2° which can be indexed to (1 1 1), (2 0 0), (2 2 0), (3 1 1), and (2 2 2), respectively, corresponding to WC_{1-x} phase (JCPDS No. 20-1316) with a face-centered cubic (fcc) structure (Fig. 3b). The patterns of the WC-800-m are related to the mixed phase of both WC_{1-x} with an fcc lattice and WC (JCPDS No. 25-1047) with a hexagonal-closed packing (hcp) lattice (Fig. 3c). As shown in Fig. 3d, the WC-900-m reveals XRD patterns related to pure WC phase with 2θ = 31.5°, 35.6°, 48.3°, 63.9°, 65.7°, 73.1°, 75.4°, and 77.1° corresponding to (0 0 1), (1 0 0), (1 0 1), (1 1 0), (0 0 2), (1 1 1), (2 0 0), and (1 0 2) respectively, representing complete transition of crystalline structure between mesoporous tungsten nitride and tungsten carbide. The phase transition of WC nanostructure from W_2N nanostructure is formed via WC_{1-x} phase according to increasing temperature. From the structural characterization, during the carburization process of the mesoporous W_2N, it is found that the W_2N is gradually carburized due to homogeneous substitution of nitrogen atoms in the metal nitride with carbon atoms without serious collapse and aggregation. In particular, it is likely that specific surface area and pore diameter of the mesoporous tungsten carbide catalysts prepared by the W_2N with fcc decrease with increasing reaction temperature due to phase transition between fcc of W_2N and hcp of WC.

In general, tungsten carbide particles are formed by a temperature programmed reaction method, which oxide precursors are placed under CH_4/H_2 atmosphere at relatively high reaction temperatures. In order to compare the tungsten carbide structures prepared in our synthetic approach with tungsten carbides (denoted as WC-600-c, WC-700-c, WC-800-c, WC-900-c, respectively) conventionally prepared at different reaction temperatures, the layered tungsten oxides were heated at 600, 700, 800, and 900 °C under CH_4/H_2 atmosphere. The WC-600-c exhibits dominant W_2C and tungsten metallic phase without WC phase (Fig. S1 of Supplementary data). With increasing reaction temperature from 700 to 900 °C, the crystal structures of the samples are transformed between W_2C and WC. In particular, the WC-900-c exhibits non-porous structure and low specific surface area of 16.5 $m^2\ g^{-1}$ in comparison with the well-defined mesoporous WC-900-m (Fig. S2 and S3 of Supplementary data).

The surface chemical states of the as-prepared mesoporous tungsten carbides were characterized by XPS analysis (Fig. S4 of Supplementary data). For the WC-700-m, WC-800-m, and WC-900-m, the $W4f_{7/2}$ and $4f_{5/2}$ peaks typically appear at around ~32 and ~34 eV, respectively, with a theoretical area ratio of 4:3. All as-prepared mesoporous tungsten carbides consist of carbide and oxidation states. In particular, the WC-900-m (85.9%) shows 1.2 times higher carbide state than the WC-800-m (71.5%) and WC-700-m (71.8%). This means that surface states of the WC-800-m and WC-700-m containing WC_{1-x} phase could be easily transformed into oxidation state by air treatment to avoid ignition of the sample during synthesis due to unstable surface state of WC_{1-x} phase in comparison with the WC-900-m containing pure WC phase [37].

3.2. Electrochemical characterization of mesoporous tungsten carbides as non-Pt catalysts

To characterize ORR properties of mesoporous tungsten carbide catalysts in alkaline solution, CVs of the samples in 0.1 M NaOH solution were obtained as shown in Fig. 4. The on-set potentials of ORR catalytic activity of the WC-700-m, WC-800-m, and WC-900-m in O_2-saturated 0.1 M NaOH are −0.250, −0.068, and −0.065 V, respectively. The reduction peaks of the WC-800-m and WC-900-m are shifted into more positive potential in the CVs as compared with

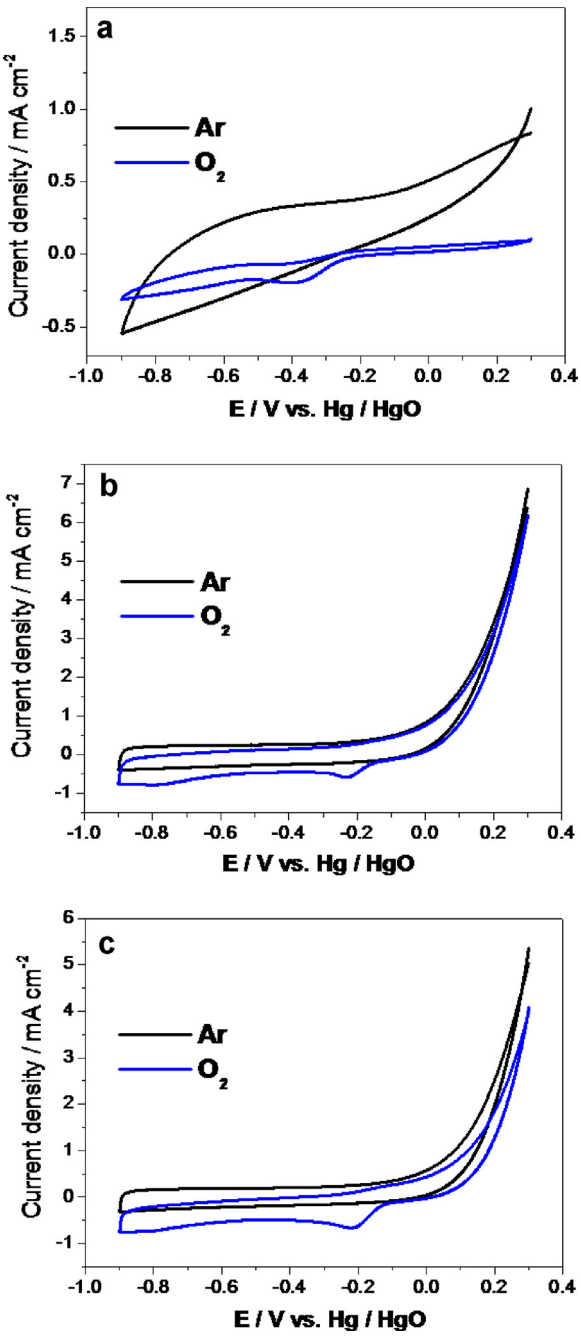

Fig. 4. CVs of WC-700-m, WC-800-m, and WC-900-m in Ar- or O_2-saturated 0.1 M NaOH with a scan rate of 50 mV s^{-1}.

that of the WC-700-m, representing that WC phase contained in the WC-800-m and WC-900-m could enhance the ORR performance.

To further compare the catalytic performance and the ORR mechanism of these catalysts, rotating ring disk electrode (RRDE) analysis was carried out as illustrated in Fig. 5. The onset potentials of the WC-800-m and WC-900-m toward ORR in the RRDE curves are significantly shifted to positive direction, as compared with the WC-700-m (Fig. 5a). The disk current density of the WC-900-m is much larger than those of the WC-700-m and WC-800-m, whereas the ring current density of the WC-900-m is comparably smaller than those of the WC-700-m and WC-800-m. The plots of the numbers of exchanged electrons (n) and generation yield (%H_2O_2) of hydrogen peroxide during ORR versus electrode potentials are as shown in Fig. 5b. The n and %H_2O_2 can be obtained according to the following equations:

$$n = \frac{4i_d}{i_d + i_r/N}$$

$$\%H_2O_2 = \frac{4-n}{2}$$

where i_d is the current on glass carbon electrode, i_r is the current on ring disk electrode, and N is the collecting coefficient number of −0.4245. The n exchanged by the WC-900-m toward ORR is determined to be ~3.9 near four electron transfer process as compared with ~3.0 and ~3.5 of the WC-700-m and WC-800-m, respectively. Furthermore, the formation of H_2O_2 during the ORR process was monitored using RRDE measurements. The %H_2O_2 generated by the WC-900-m is much lower (~10%) than that by the WC-700-m and WC-800-m (about 20–40%). Thus, we can suggest that a highly improved electrochemical activity of the WC-900-m may result from more exposed carbide states as an active site as compared to the WC-800-m and WC-700-m, which is in good agreement with the XPS data. Furthermore, the ORR activity of the mesoporous WC-900-m in O_2 saturated 0.1 M NaOH is much superior to that of the WC-900-c conventionally prepared at 900 °C in CH_4/H_2 (Fig. S5 of Supplementary data). Recently, Lin et al. reported the tungsten carbide-based nanocomposites as an efficient electrochemical catalyst for oxygen reduction reaction in alkaline electrolyte [38]. However, the nanosized-tungsten carbide reported by Lin et al. show low ORR activity (−0.304 V as half wave potential) and number of exchanged electrons (~3.25) compared to WC-900-m nanostructure. As a result, among the WC catalysts, the WC-900-m exhibits an improved ORR activity due to catalytic properties of WC phase, dominant carbide surface state, and porous electrode structure.

3.3. Characterization of Pd NPs deposited on mesoporous tungsten carbide

To further enhance an oxygen reduction activity of the WC-900-m comparable to conventional Pt catlayst, we synthesized Pd NPs (4 wt.%) deposited on the mesoporous WC-900-m (Pd/WC-900-m) using a borohydride reduction method at 25 °C (Fig. S6 of Supplementary data). Also, electrochemical active surface areas (EASAs) of two catalysts were measured by integrating the charges on the reduction of the oxide film regions [39]. The EASAs are 79.01 and 55.865 m^2 g^{-1} for the Pd/WC-900-m and Pt/C, respectively. This represents that the Pd/WC-900-m have a high electrochemical active surface area due to high dispersion of Pd (4 wt.%) nanoparticles on WC-900-m with high surface area. In Fig. 6a–c, the current densities of the WC-900-m, Pd/WC-900-m, and Pt/C at −0.1 V are 1.694, 2.861, and 2.802 mA/cm^2, respectively. The Pd/WC-900-m as non-Pt catalyst exhibits similar electrochemical reduction activity comparable to that of the Pt/C. The improved electrochemical activity of Pd/WC-900-m may be attributed to synergy effect by the higher EASAs of Pd NPs as major catalyst and the catalytic behavior of WC in ORR. Furthermore, to compare an electrocatalytic stability for the ORR, the stability test of the catalysts was carried out by applying linear potential sweep between −0.4 and +0.1 V for 2,000 cycles in O_2-saturated 0.1 M NaOH solution at 25 °C. The Pd/WC-900-m exhibits an activity loss of 13.1% in ORR current density at −0.1 V after stability test, whereas the Pt/C exhibits a considerable loss of 38.0% in ORR current density (Fig. 6b and c). Furthermore, in the half wave potential region, the Pd/WC-900-m exhibits a slight potential drop of 13 mV at a half wave current density of −2 mA/cm^2 after 2,000 cycles, whereas the Pt/C exhibits a considerable drop of 30 mV after stability test (Fig. 6d). The WC as a support material has been well known to exhibit higher electrochemical

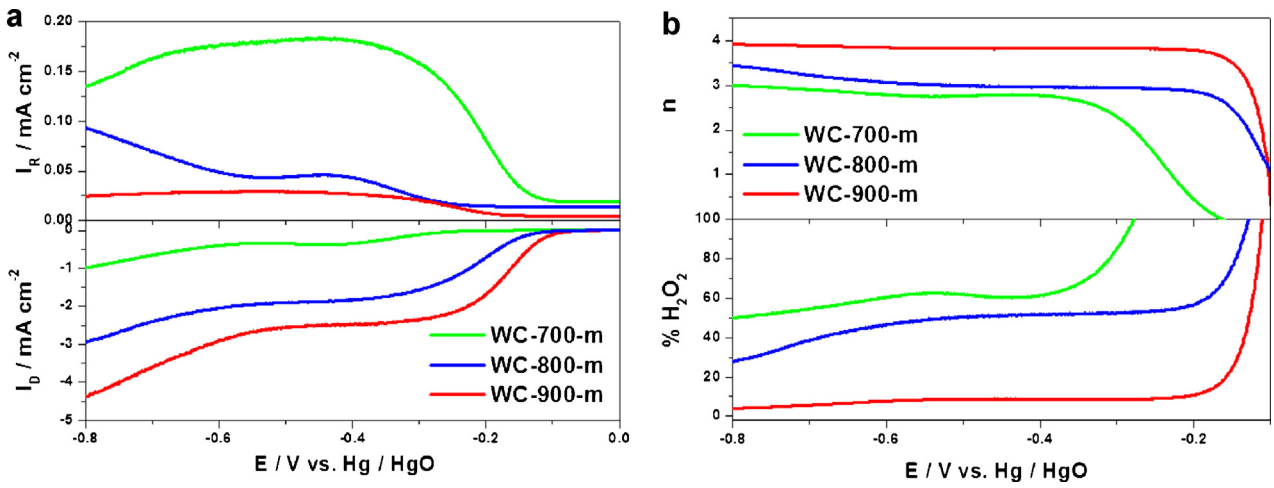

Fig. 5. (a) Polarization curves of WC-700-m, WC-800-m, and WC-900-m in O_2-saturated 0.1 M NaOH with a potential scan rate of 5 mV s^{-1} and an electrode rotation rate of 1600 rpm. The ring potential was maintained at 0.4 V. (b) Calculated values of n and $\%H_2O_2$ of the as-prepared catalysts for ORR.

stability as anodic or cathodic electrode in alkaline electrolyte fuel cells [40,41]. In particular, Fu et al. reported that metal-tungsten carbide nanostructures exhibit improved electrochemical stability due to the strong covalent interaction between metallic catalysts and WC substrates [42]. Accordingly, the improved electrochemical stability of the Pd/WC-900-m might result from strong interaction among Pd catalysts and WC supports. As a result, we found remarkably improved electrochemical properties of the Pd/WC-900-m for

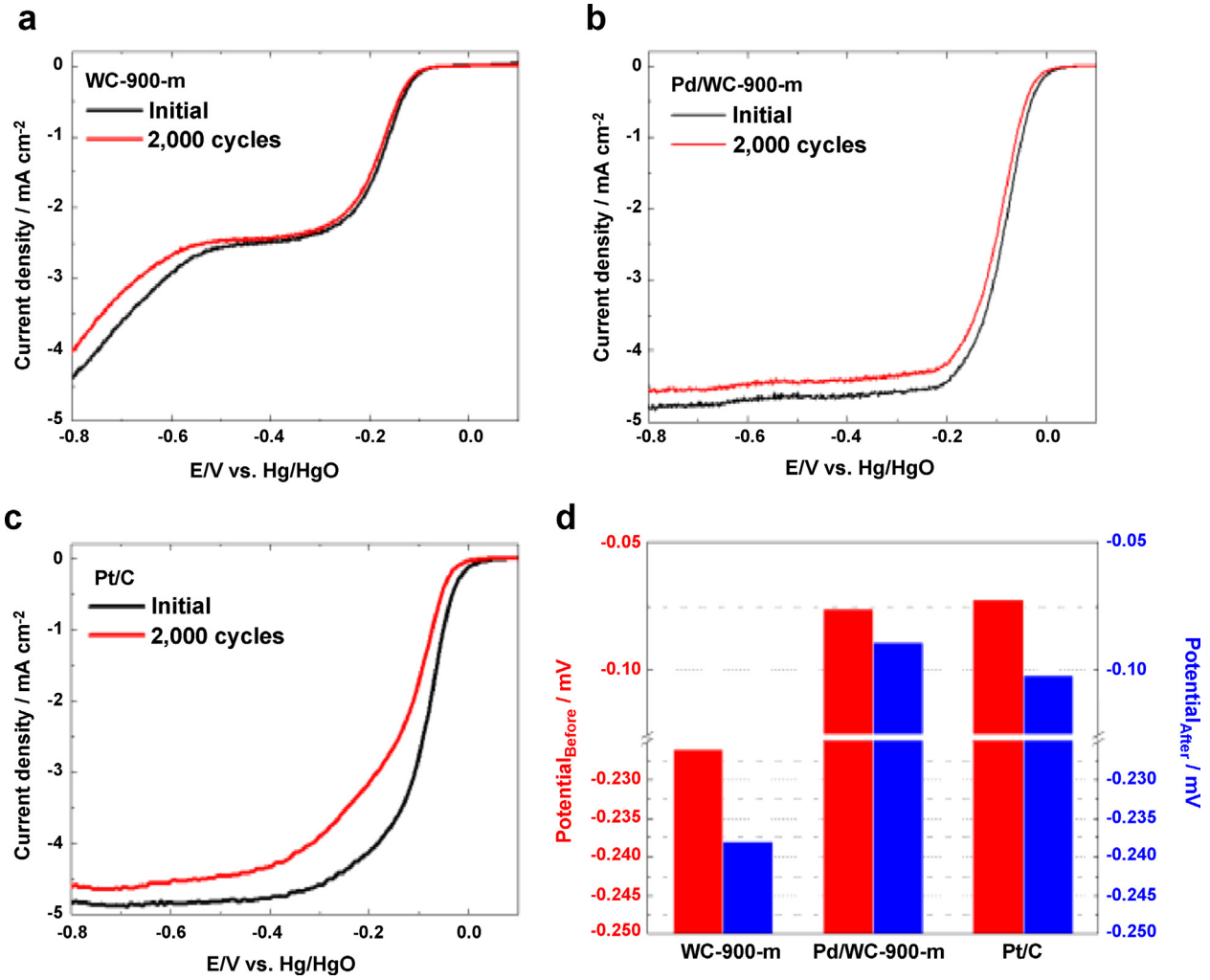

Fig. 6. ORR polarization curves of (a) WC-900-m, (b) Pd/WC-900-m, and (c) Pt/C with a scan rate of 5 mV s^{-1} and an electrode rotation rate of 1600 rpm in O_2-saturated 0.1 M NaOH solution at 25 °C. (d) Comparison of half wave potenials of the WC-900-m, Pd/WC-900-m, and Pt/C before and after stability test. The stability test was carried out by applying linear potential sweeps between −0.4 and 0.1 V for 2000 cycles with a scan rate of 50 mV s^{-1} in O_2-saturated 0.1 M NaOH solution at 25 °C.

oxygen reduction reaction in alkaline electrolyte. Thus, the Pd/WC-900-m can be utilized as a promising cathode in alkaline fuel cell applications.

4. Conclusions

We have successfully synthesized well-defined mesoporous tungsten carbide catalysts using layered W_2N nanoparticles. The tungsten carbides derived from W_2N nanoparticles at different reaction temperatures in CH_4/H_2 mixture atmosphere exhibit isothermal mesoporous characteristics and fairly homogeneous pore size distributions. During the carburization process using the layered W_2N, the WC phase can be completely obtained by carburizing W_2N nanoparticles without serious collapse and aggregation. The particular catalytic properties of WC phase and mesoporous structure with large active surface area in the WC-900-m might lead to the enhanced electrocatalytic properties such as ORR activity in an alkaline solution. Furthermore, the Pd/WC-900-m exhibited much enhanced electrochemical oxygen reduction properties in comparison with conventional Pt catalyst.

Acknowledgments

This work was supported by the National Research Foundation of Korea Grant funded by the Korean Government (NRF-2012M1A2A2671689) and the International Collaborative Energy Technology R&D Program of the Korea Institute of Energy Technology Evaluation and Planning (KETEP), granted financial resource from the Ministry of Trade, Industry & Energy, Republic of Korea. (No. 2138520030800).

Appendix A. Supplementary data

Supplementary material related to this article can be found, in the online version, at http://dx.doi.org/10.1016/j.apcata.2014.02.034.

References

[1] A. Brouzgou, A. Podias, P. Tsiakaras, J. Appl. Electrochem. 43 (2013) 119–136.
[2] F.H. Ribeiro, R.A. Dalla Betta, G.J. Guskey, M. Boudart, Chem. Mater. 3 (1991) 805–812.
[3] S. Ted Oyama, J.C. Schlatter, J.E. Metcalfe III, J.M. Lambert Jr., Ind. Eng. Chem. Res. 27 (1988) 1639–1648.
[4] J.G. Chen, Chem. Rev. 96 (1996) 1477–1498.
[5] K. Lee, A. Ishihara, S. Mitsushima, N. Kamiya, K.-I. Ota, Electrochim. Acta 49 (2004) 3479–3485.
[6] A. Serov, C. Kwak, Appl. Catal. B-Environ. 90 (2009) 313–320.
[7] E.C. Weigert, A.L. Stottlemyer, M.B. Zellner, J.G. Chen, J. Phys. Chem. C 111 (2007) 14617–14620.
[8] M.K. Jeon, H. Daimon, K.R. Lee, A. Nakahara, S.I. Woo, Electrochem. Commun. 9 (2007) 2692–2695.
[9] Y. Hara, N. Minami, H. Matsumoto, H. Itagaki, Appl. Catal. A-Gen. 332 (2007) 289–296.
[10] A-R. Ko, J.-Y. Kim, J.-K. Oh, H.-S. Kim, Y.-W. Lee, S.-B. Han, K.-W. Park, Phys. Chem. Chem. Phys. 12 (2010) 15181–15183.
[11] H. Meng, P.K. Shen, J. Phys. Chem. B 109 (2005) 22705–22709.
[12] E. Antolini, Appl. Catal. B-Environ. 74 (2007) 337–350.
[13] Y.-W. Lee, A-R. Ko, S.-B. Han, H.-S. Kim, D.-Y. Kim, S.-J. Kim, K.-W. Park, Chem. Commun. 46 (2010) 9241–9243.
[14] H.J. Kim, H.-S. Park, D.J. Suh, ChemSusChem 2 (2009) 221–225.
[15] A. Brouzgou, S.Q. Song, P. Tsiakaras, Appl. Catal. B-Envion. 127 (2012) 371–388.
[16] S. Seraji, Y. Wu, M.J. Forbess, S.J. Limmer, T. Chou, G. Cao, Adv. Mater. 12 (2000) 1695–1698.
[17] C. Ma, N. Brandon, G. Li, J. Phys. Chem. C 111 (2007) 9504–9508.
[18] J.A. Nelson, M.J. Wagner, Chem. Mater. 14 (2002) 1639–1642.
[19] D. Liu, B.B. Garcia, Q. Zhang, Q. Guo, Y. Zhang, S. Sepehri, G. Cao, Adv. Funct. Mater. 19 (2009) 1015–1023.
[20] L. Volpe, M.J. Boudart, Solid State Chem. 59 (1985) 332–347.
[21] F. Schüth, W. Schmidt, Adv. Mater. 14 (2002) 629–638.
[22] A. Taguchi, F. Schüth, Microporous Mesoporous Mat. 77 (2005) 1–45.
[23] P. Kumar, V.V. Guliants, Microporous Mesoporous Mat. 132 (2010) 1–14.
[24] J.C. Groen, L.A.A. Peffer, J. Pérez-Ramírez, Microporous Mesoporous Mat. 60 (2003) 1–17.
[25] T. Yu, Y.H. Deng, L. Wang, R.L. Liu, L.J. Zhang, B. Tu, D.Y. Zhao, Adv. Mater. 19 (2007) 2301–2306.
[26] Z. Hong, M. Wei, T. Lan, L. Jiang, G. Cao, Energy Environ. Sci. 5 (2012) 5408–5413.
[27] Y.-S. Jun, W.H. Hong, M. Antonietti, A. Thomas, Adv. Mater. 21 (2009) 4270–4274.
[28] H.-Y. Lin, H.-C. Huang, W.-L. Wang, Microporous Mesoporous Mat. 115 (2008) 568–575.
[29] T. Hisatomi, M. Otani, K. Nakajima, K. Teramura, Y. Kako, D. Lu, T. Takata, J.N. Kondo, K. Domen, Chem. Mater. 22 (2010) 3854–3861.
[30] Y. Hara, N. Minami, H. Itagaki, Appl. Catal. A-Gen. 323 (2007) 86–93.
[31] Z. Wu, Y. Yang, D. Gu, Q. Li, D. Feng, Z. Chen, B. Tu, P.A. Webley, D. Zhao, Small 5 (2009) 2738–2749.
[32] K. Nakajima, T. Fukui, H. Kato, M. Kitano, J.N. Kondo, S. Hayashi, M. Hara, Chem. Mater. 22 (2010) 3332–3339.
[33] L. Hu, S. Ji, Z. Jiang, H. Song, P. Wu, Q. Liu, J. Phys. Chem. C 111 (2007) 15173–15184.
[34] J. Chen, C. Burger, C.V. Krishnan, B. Chu, J. Am. Chem. Soc. 127 (2005) 14140–14141.
[35] P. Krawiec, P.L. De Cola, R. Gläser, J. Weitkamp, C. Weidenthaler, S. Kaskel, Adv. Mater. 18 (2006) 505–508.
[36] L. Hu, S. Ji, T. Xiao, C. Guo, P. Wu, P. Nie, J. Phys. Chem. B 111 (2007) 3599–3608.
[37] K.M. Reddy, T.N. Rao, J. Joardar, Mater. Chem. Phys. 128 (2011) 121–126.
[38] C.K. Poh, S.H. Lim, Z. Tian, L. Lai, Y.P. Feng, Z. Shen, J. Lin, Nano Energy 2 (2013) 28–39.
[39] S.S. Mahapatra, J. Datta, Int. J. Electrochem. 2011 (2011) 563495.
[40] R.H. Wang, Y. Xie, Y.K. Shi, J.Q. Wang, C.G. Tian, P.K. Shen, H.G. Fu, Chem. Eur. J. 18 (2008) 7443–7451.
[41] R.H. Wang, C.G. Tian, L. Wang, B.L. Wang, H.B. Zhang, H.G. Fu, Chem. Commun. 45 (2009) 3104–3106.
[42] J. Yang, Y. Xie, R. Wang, B. Jiang, C. Tian, G. Mu, J. Yin, B. Wang, H. Fu, ACS Appl. Mater. Inter. 5 (2013) 6571–6579.